The Impact of Non-Neural Sources on Aperiodic EEG Activity

AUTHORS:

Marius Tröndle[1] *, Nicolas Langer[1]

AFFILIATIONS:

1: Methods of Plasticity Research, Department of Psychology, University of Zurich, Zurich, Switzerland

CORRESPONDING AUTHOR(*):

Marius Tröndle

Methods of Plasticity Research

Department of Psychology

University of Zurich

Binzmühlenstrasse 14

CH-8050, Zürich, Switzerland

E-mail: m.troendle@psychologie.uzh.ch, Tel.: +41 44 634 58 88

Abstract

Aperiodic, 1/f-like EEG activity is increasingly used to investigate neural dynamics in cognitive and clinical research, with applications ranging from experimental manipulations to clinical biomarker development. However, these applications assume, without systematic testing, that aperiodic parameters primarily reflect neural activity rather than non-neural sources. To address this critical gap, we systematically quantified how data quality and physiological artifacts influence aperiodic parameter estimation across two independent datasets (N=99 and N=103) using complementary methodological approaches.

Poor data quality and ocular artifacts significantly increased aperiodic offsets and exponents, whereas muscular artifacts showed opposite effects. These spatially widespread effects reached magnitudes comparable to neurophysiologically meaningful group differences and were only partially attenuated by state-of-the-art preprocessing. Cardiac artifacts showed modest effects limited to the offset. Critically, regression-based statistical correction effectively mitigated artifact-induced biases.

Our findings establish that differential artifact rates between experimental conditions or populations can substantially bias neural interpretations of aperiodic parameters and provide methodological guidelines for ensuring valid inference.

Introduction

Electroencephalography (EEG) has emerged as a powerful tool for understanding brain function in health and disease. Beyond the well-characterized periodic, or oscillatory activity, recent work highlights that EEG signals also contain substantial aperiodic, or non-oscillatory, activity[1,2]. In the frequency domain, this aperiodic activity manifests as a continuous background signal that exhibits 1/f-like power law scaling, meaning that power decreases as frequency increases. This characteristic scaling pattern is ubiquitous across neurophysiological recordings, but was historically dismissed as background noise. The growing recognition that aperiodic activity carries physiologically meaningful information, together with advances in computational methods for separating periodic and aperiodic signal components, has catalyzed a paradigm shift driving systematic investigations of aperiodic activity across diverse cognitive and clinical research domains.

Two parameters characterize aperiodic activity: the aperiodic offset, reflecting broadband power shift, and the exponent, describing spectral steepness. Despite extensive research, the neural origins of these parameters remain uncertain. The aperiodic offset has been linked to neuronal population spiking activity[3], whereas variations in the exponent have been proposed to reflect differences in neural noise[4,5], self-organized criticality[6–8], or the most prominently[9], the balance between inhibitory and excitatory synaptic activity[10,11]. Empirically, aperiodic activity shows robust associations with age-related changes[12–14], task-related neural dynamics[15–17], and clinical status, showing alterations in autism spectrum disorders (ASD)[18,19], schizophrenia[20,21], attention-deficit/hyperactivity disorder (ADHD)[22,23], and neurodegenerative diseases[24–26]. These effects position aperiodic metrics as promising biomarkers that could inform diagnosis and treatment monitoring, an application whose success critically depends on the valid neural interpretation of aperiodic parameters.

However, a critical assumption underlies these interpretations: that extracted aperiodic parameters primarily reflect neural processes. Yet, EEG recordings, by nature, are

contaminated by physiological artifacts, typically arising from ocular movements, muscular activity, and cardiac function, as well as measurement noise from environmental and technical sources[27], which can distort spectral estimates. First studies suggest that these confounds extend to aperiodic parameter estimates. A recent machine learning approach showed that aperiodic EEG features discriminate between high and low quality data segments[28], indicating sensitivity of aperiodic parameters to data quality. While this finding indicates a potential contamination, it remains unknown how specific artifact sources and variations in data quality systematically affect aperiodic parameter estimates. Only one study has directly implicated cardiac artifacts[29], leaving a comprehensive assessment lacking.

This knowledge gap is critical as aperiodic metrics gain traction in clinical research[9]. Well-documented differences in data quality or artifact prevalence between patient and control groups[30,31] - or even between experimental conditions - can bias aperiodic parameter estimates and confound their neural interpretation**.** Without a systematic understanding of the sources and magnitudes of these influences, it remains uncertain whether reported group differences reflect genuine neural variation or systematic non-neural contamination. Beyond clinical applications, distinguishing neural from non-neural contributions to aperiodic activity has substantial theoretical implications. Many of the empirical patterns are cited as evidence for shifts in excitation/inhibition balance[9,17,32], but could instead reflect differences in physiological artifacts or recording quality. Understanding and accounting for these influences is therefore essential for advancing our fundamental understanding of what aperiodic parameters represent.

To address this challenge, we systematically quantified how data quality and physiological artifacts influence aperiodic parameter estimation in resting-state EEG. We analyzed two independent datasets with complementary approaches (Figure 1). First, we assessed the impact of data quality metrics on aperiodic parameters (Figure 1, green box). Second, we examined how ocular, muscular, and cardiac activity artifacts alter aperiodic estimates (Figure 1, blue boxes). We implemented two complementary methodologies: a *component*

retention approach, selectively removing or retaining independent components (ICs) linked to specific artifacts, and an *incremental contamination* approach, where artifact-containing segments were systematically mixed into otherwise clean data at predefined levels (illustrated in the lower blue box of Figure 1)

Together, these analyses provide the first systematic quantification of how data quality and physiological artifacts shape aperiodic parameter estimates. The results clarify the non-neural contributions to aperiodic activity and establish methodological guidelines for robust interpretation of basic and clinical research.

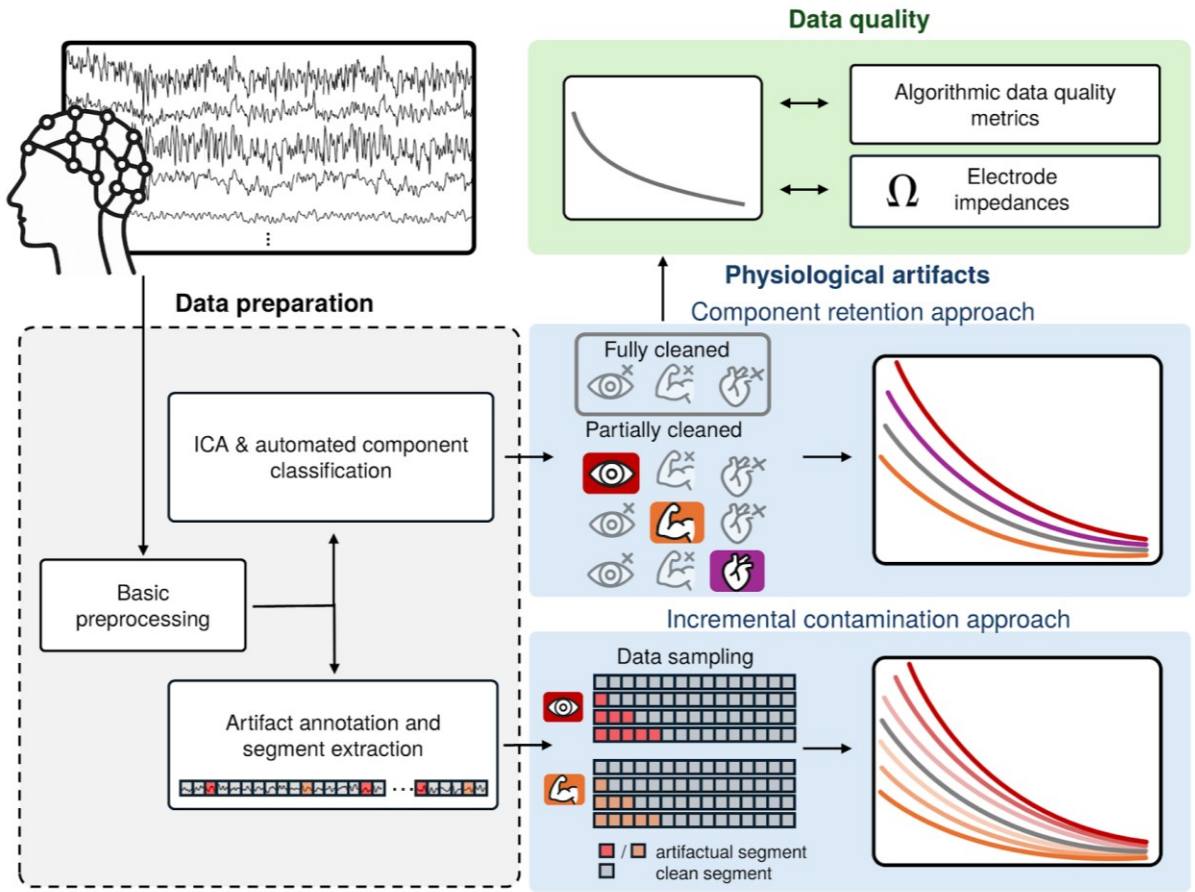

Figure 1: Overview of analyses on data quality and physiological artifacts. Schematic overview of the two analysis sets assessing the impact of data quality (green box) and physiological artifacts (blue boxes) on estimated aperiodic parameters. Basic preprocessing (gray box) included 0.5 Hz high pass filtering and removal of bad channels and of line noise. For data quality analyses, the aperiodic parameters were computed from fully cleaned EEG data (all artifactual ICs removed; green box, left). In the component retention approach, faded or crossed physiological artifact symbols indicate that the corresponding ICs were removed, whereas colored symbols denote retained ICs used for aperiodic parameter estimation (blue box, right). In the incremental contamination approach, contamination levels of 0, 1, 3, or 5 artifact segments (of 15 total), were introduced before aperiodic computation. Note that in this approach, cardiac artifacts can not be investigated (see Methods).

Results

Final sample characteristics

To enhance the robustness and generalizability of our findings, we analyzed two EEG datasets (N = 99 and N = 103) recorded with different hardware: a main dataset (electrolyte gel based EEG system), newly collected for this investigation and including eye-tracking, EMG, and ECG to improve the identification of physiological artifacts, and an independent validation dataset (saline based EEG system) previously recorded in our laboratory, which featured comparable EEG and eye-tracking data but did not include EMG or ECG recordings.

After excluding low-quality recordings at the end of preprocessing, the final samples comprised 89 participants in the main dataset (age range 18.1 to 38.7 years, sd=3.8, 67 female), and 93 participants in the validation dataset (age range 19.7 to 32.2 years, sd = 3.0, 57 female). Sample sizes for specific analysis varied depending on the availability of electrode impedance measures and the identification of artifacts. A detailed overview of both datasets and the subsamples used for different analyses is provided in Supplement 1. Additional details on the number of artifactual ICs and contaminated data segments per participant are provided in Supplement 2.

Findings were generally consistent across datasets. For clarity, statistical results are reported for both, but visualizations in the main text are limited to the main dataset, which offers more comprehensive data coverage across analyses and improved artifact detection. Full cross-dataset visualizations are presented in Supplement 3.

Effect of data quality metrics on the aperiodic signal component

We examined the relationship between data quality and the aperiodic parameter estimates using both a hardware-based measure (electrode impedances) and three algorithmic quality metrics: proportion of overall high amplitude datapoints (OHA), proportion of timepoints of high variance (THV), and proportion of channels of high variance (CHV) (see Methods for details).

Importantly, aperiodic parameters and algorithmic quality metrics were estimated from fully cleaned data (i.e. after removal of all ICs identified as artifacts by ICLabel[33]) to assess whether effects of data quality persisted after applying state-of-the-art preprocessing methods (see Figure 1).

Hardware based quality metrics: Electrode impedances

Electrode impedances were not significantly related to the aperiodic exponent in either dataset. However, statistical analyses revealed significant associations with the aperiodic offset in the main dataset, with a similar but non-significant trend in the validation dataset (see Table 1). The discrepancy likely reflects the greater statistical power of the main dataset (N = 89 vs. 55, see Supplement 1). As shown in the topographical maps (Figure 2B), this association is positive and broadly distributed across the scalp.

Algorithmic quality metrics

Analyses of the three algorithmic quality measures (OHA, CHV, THV) yielded highly consistent results across both datasets. Higher values, reflecting poorer data quality, were significantly associated with higher aperiodic offsets in the main and the validation dataset (see Table 1). This effect was widespread across the scalp (Figure 2E).

Statistical analyses further revealed significant associations between algorithmic quality metrics and the aperiodic exponent in both datasets (see Table 1). The only exception was CHV, which showed no significant effect in the main, and a marginal effect in the validation dataset (cluster p = 0.028, slightly above the two-sided threshold of p = 0.025). As shown in Figure 2F, these associations were strongest over parietal and occipital regions, indicating that poorer data quality is linked to a steeper aperiodic signal component.

Table 1

Statistical results (Cluster-based permutation tests, CBPTs): Effect of data quality metrics on the aperiodic signal parameters.

	Aperiodic offset (avg. standardized β, cluster p)		Aperiodic exponent (avg. standardized β, cluster p)	
	Main dataset	Validation dataset	Main dataset	Validation dataset
Electrode impedance	β=0.31, p≤0.001	β=0.40, p=0.100	β=0.26, p=0.115	β=-0.33, p=0.250
OHA	β=0.40, p≤0.001	β=0.48, p≤0.001	β=0.29, p=0.009	β=0.30, p≤0.001
THV	β=0.35, p≤0.001	β=0.51, p≤0.001	β=0.24, p=0.003	β=0.29, p=0.003
CHV	β=0.30, p≤0.001	β=0.34, p≤0.001	β=0.23, p=0.100	β=0.25, p=0.028

Note: Standardized β's are averaged across all electrodes of the significant cluster. If no cluster was significant, β's are averaged across the largest non-significant cluster.

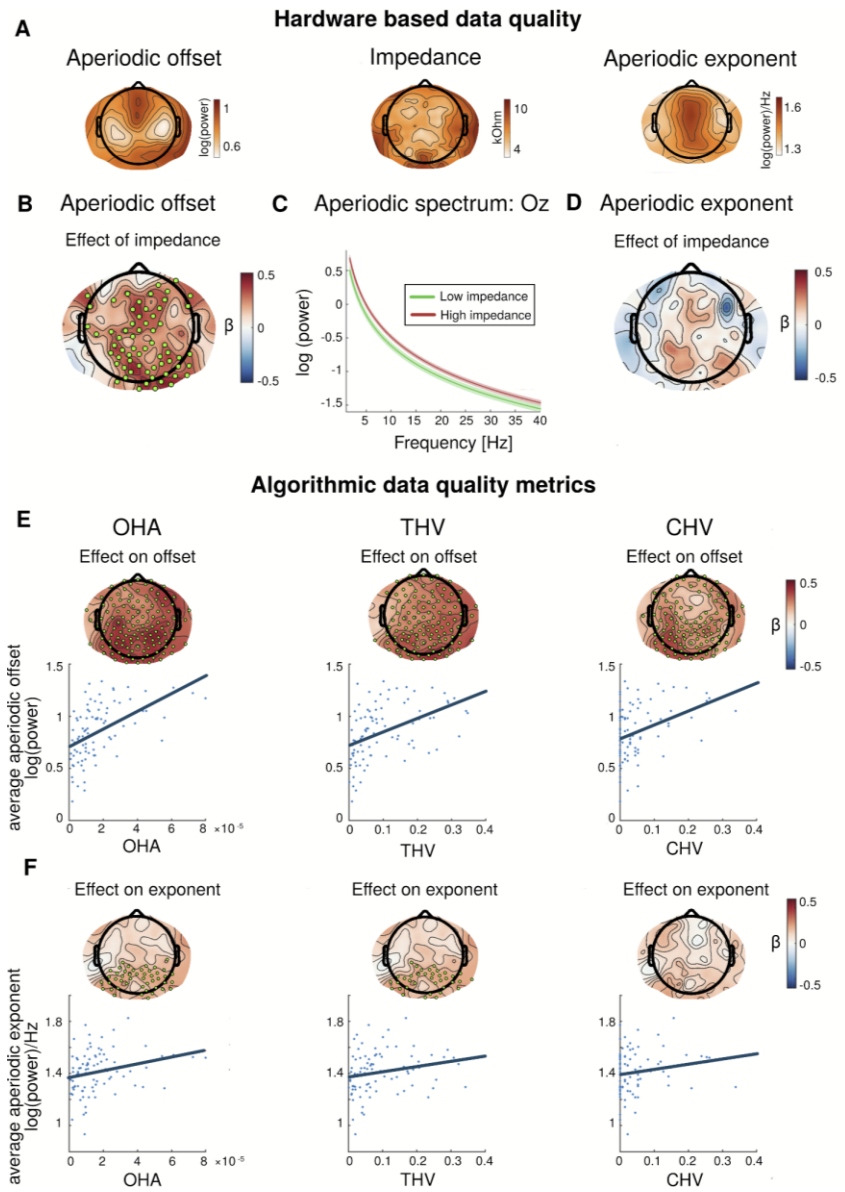

Figure 2: Effects of data quality on aperiodic parameter estimation. Results are shown for the main dataset. Panels A-D illustrate effects of electrode impedances on the aperiodic offset and exponent. Panel A shows the topographical distribution of the aperiodic offset, exponent, and the impedances. Panels B&D display standardized β's from linear regressions predicting the aperiodic parameters from electrode impedances, green dots mark significant electrode clusters by the CBPT. Panel C presents median-split aperiodic spectra at electrode Oz, shaded areas indicate standard error of the mean. Panels E-F depict the effects of algorithmic quality metrics (OHA THV, CHV) on the aperiodic parameters. Topographies show standardized β coefficients, with green dots indicating significant electrodes of the CBPTs. Scatterplots below display average aperiodic parameters (across electrodes) predicted by the quality metrics, with dark blue lines representing least-squares fits.

Effect of physiological artifacts on the aperiodic signal component

We next examined how physiological artifacts influence the aperiodic parameter estimation using two complementary approaches illustrated in Figure 1 (blue boxes). Strikingly, both the component retention and incremental contamination methods yielded highly consistent results across datasets.

Ocular artifacts

In the component retention approach, ocular contamination significantly affected both the aperiodic offset and the aperiodic exponent (Table 2). Ocular artifacts were associated with larger offsets and steeper aperiodic slopes. Crucially, these effects were not restricted to prefrontal electrodes near the eyes, but extended to temporal, parietal, and occipital regions (Figure 3B and 3D). Thus, eye movements alter the aperiodic signal across the scalp even during eye-closed resting-state recordings. As expected, these effects were amplified in the eyes-open data (see Supplement 4).

The incremental contamination approach further confirmed these findings. Using co-registered eye-tracking data to identify ocular events, we separately assessed blinks and saccades, an analysis not possible with automated IC classification. Both blinks and saccades significantly increased the aperiodic offset and exponent, with blinks exerting stronger effects (Table 2), producing steeper aperiodic signal components with larger offsets (Figure 3E-3J).

Finally, supplementary analyses (Supplement 5) demonstrated that blink and saccade-related effects largely persisted even after removal of all ICs identified as artifacts, indicating that standard preprocessing may not fully eliminate ocular influences on the aperiodic estimates. Consequently, ocular activity may still confound neural interpretations of aperiodic parameters, despite conventional artifact correction.

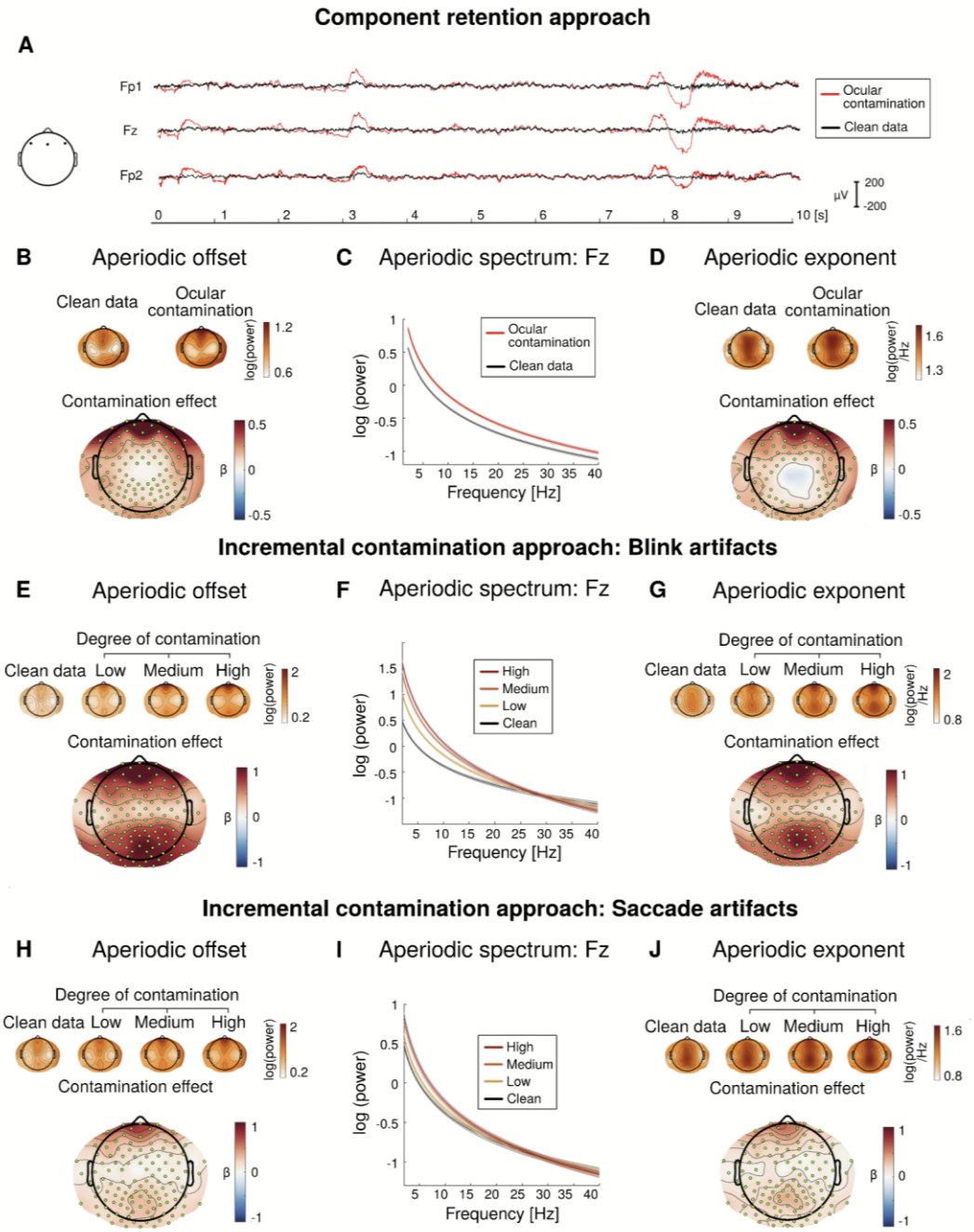

Figure 3: Effects of ocular artifact contamination on aperiodic parameter estimation. Results are shown for the main dataset. Panels A-D illustrate findings from the component retention approach. Panel A shows data from three prefrontal electrodes (left: Fp1, middle:Fz, right: Fp2) before and after removal of ICs classified as ocular activity. Small topographies on top of B&D display aperiodic parameters derived from fully cleaned data (all artifactual ICs removed) and partially cleaned (ocular ICs retained) data. Larger maps display standardized regression coefficients from linear mixed-effects models predicting aperiodic parameters from ocular contamination; green dots mark electrodes significant in CBPT. Panel C shows mean aperiodic spectra for fully cleaned versus ocular contaminated data, with shaded areas

indicating standard error of the mean. Panel E-J present results from the incremental contamination approach for blinks and saccades, using the same visualization schemes as B-D. Contamination effects are illustrated by contrasting clean data (0 artifactual segments) vs. medium contaminated data (3 out of 15 artifactual segments).

Table 2

Statistical results (CBPTs): Effect of physiological artifact contamination on the aperiodic offset and exponent.

	Aperiodic offset (avg. standardized β, cluster p)		Aperiodic exponent (avg. standardized β, cluster p)	
	Main dataset	Validation dataset	Main dataset	Validation dataset
Ocular artifacts				
Component retention	β=0.21, p≤0.001	β=0.28, p≤0.001	β=0.21, p≤0.001	β=0.22, p≤0.001
Incremental contamination: Blinks	β=0.66, p≤0.001	β=0.88, p≤0.001	β=0.53, p≤0.001	β=0.74, p≤0.001
Incremental contamination: Saccades	β=0.21, p≤0.001	β=0.36, p≤0.001	β=0.18, p≤0.001	β=0.28, p≤0.001
Muscular artifacts				
Component retention	β=−0.11, p≤0.001	β=−0.09, p≤0.001	β=−0.27, p≤0.001	β=−0.24, p≤0.001
Incremental contamination: EEG based	β=−0.08, p=0.017	β=0.05, p=0.086	β=−0.19, p≤0.001	β=−0.17, p≤0.001
Incremental contamination: EMG based	β=0.06, p=0.157	n.a.	β=−0.14, p≤0.001	n.a.
Cardiac artifacts				
Component retention	β=0.03, p≤0.001	β=0.08, p≤0.001	p=0.04, β=0.02	p=0.067, β=0.04

Note: For the incremental contamination approach, p values refer to the significance of the contamination factor in the linear mixed model. Standardized β's refer to the contrast "medium contamination vs. no contamination" and are averaged across all electrodes of the significant cluster. If no cluster was significant, β's are averaged across the largest non-significant cluster. n.a. indicates that the analysis was not applicable to the dataset.

Muscular artifacts

In the component retention approach, muscular artifacts significantly affected both the aperiodic offset and the aperiodic exponent in both datasets (see Table 2). In contrast to the findings for data quality and ocular artifacts, muscular contamination led to a decrease in the aperiodic offset and a flattening of the aperiodic component. These effects were not restricted to specific electrodes but were observed broadly across the scalp (Figure 4B and 4D).

The incremental contamination approach confirmed these findings using two artifacts detection methods: An established EEG-based algorithm[34] (both datasets) and EMG-based detection (main dataset only). Robust effects on the aperiodic exponent were observed across methods (Table 2). Similar trends were seen for the offset (Figure 4E), reaching statistical significance only with the EEG-based detection in the main dataset (Table 2; Supplement 6).

Consistent with ocular artifact results, muscular contamination effects on the aperiodic exponent persisted even when using the fully cleaned data, i.e., time windows identified in basic preprocessed data, but aperiodic parameters computed after ICA-based artifact removal (Supplement 5), reinforcing concerns about artifact-induced misinterpretation of aperiodic signal components despite applying well-established artifact correction methods.

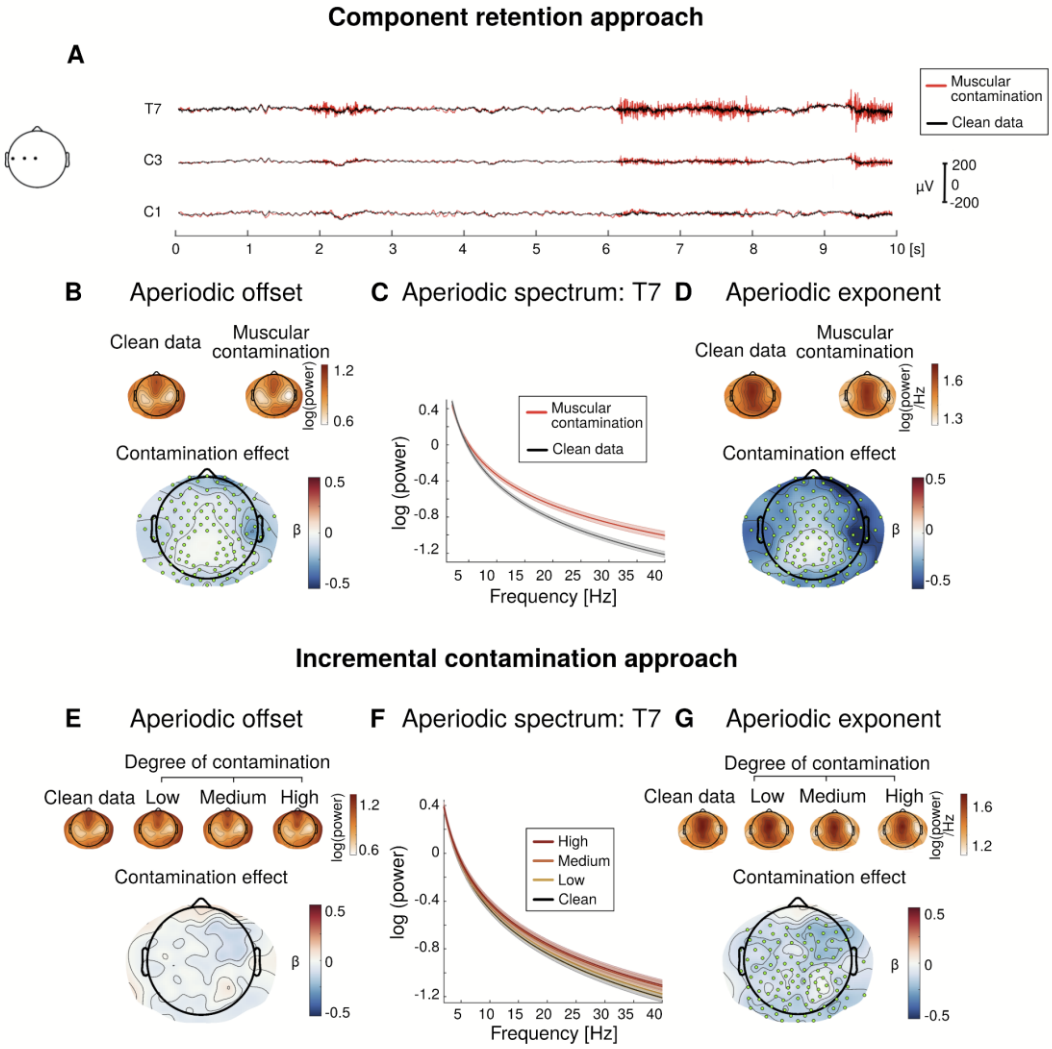

Figure 4: Effects of muscular artifact contamination on aperiodic parameter estimation. Results are shown for the main data set. Panels A-D illustrate findings from the component retention approach. Panel A shows prototypical data from three centrotemporal electrodes (from left to right: T7, C3 and C1) before and after the removal of ICs identified as muscular activity. Small topographies above B and D display aperiodic parameters derived from fully cleaned data (all artifactual ICs removed) and partially cleaned data, (muscular ICs retained). Larger maps show standardized regression coefficients from the linear mixed effects models predicting the aperiodic parameters from muscular contamination; green dots indicate electrodes significant in CBPT. Panel C shows mean aperiodic spectra for fully cleaned data versus data in which muscular ICs were retained, with shaded areas indicating the standard errors of the mean. Panels E-G presents results from the incremental contamination approach using direct EMG-artifact detection. Contamination effects are illustrated by contrasting clean data (0 artifactual segments) vs. medium contaminated data (3 out of 15 artifactual segments).

Cardiac artifacts

Results regarding cardiac artifacts should be interpreted with caution. First, the available sample size was smaller than in the other analysis (main dataset: N = 56 , validation dataset: N = 35), as ICA did not identify cardiac ICs in a substantial proportion of participants (Supplement 1 & 2). Second, the incremental contamination approach could not be applied because typical resting heart rate of healthy adults (60 and 90 beats per minute[35]) precludes the extraction of artifact-free one-second segments.

In the component retention approach, cardiac artifact contamination was associated with a significant increase of the aperiodic offset across both datasets, with effects broadly distributed across the scalp (Figure 5B). Notably, this effect was evident in within-participant analyses (Figure 5B) but absent in between-subject comparisons (Figure 5C). For the aperiodic exponent, a marginal positive relationship with cardiac contamination was observed, but it did not reach the significance threshold of $p<0.025$ (Table 2).

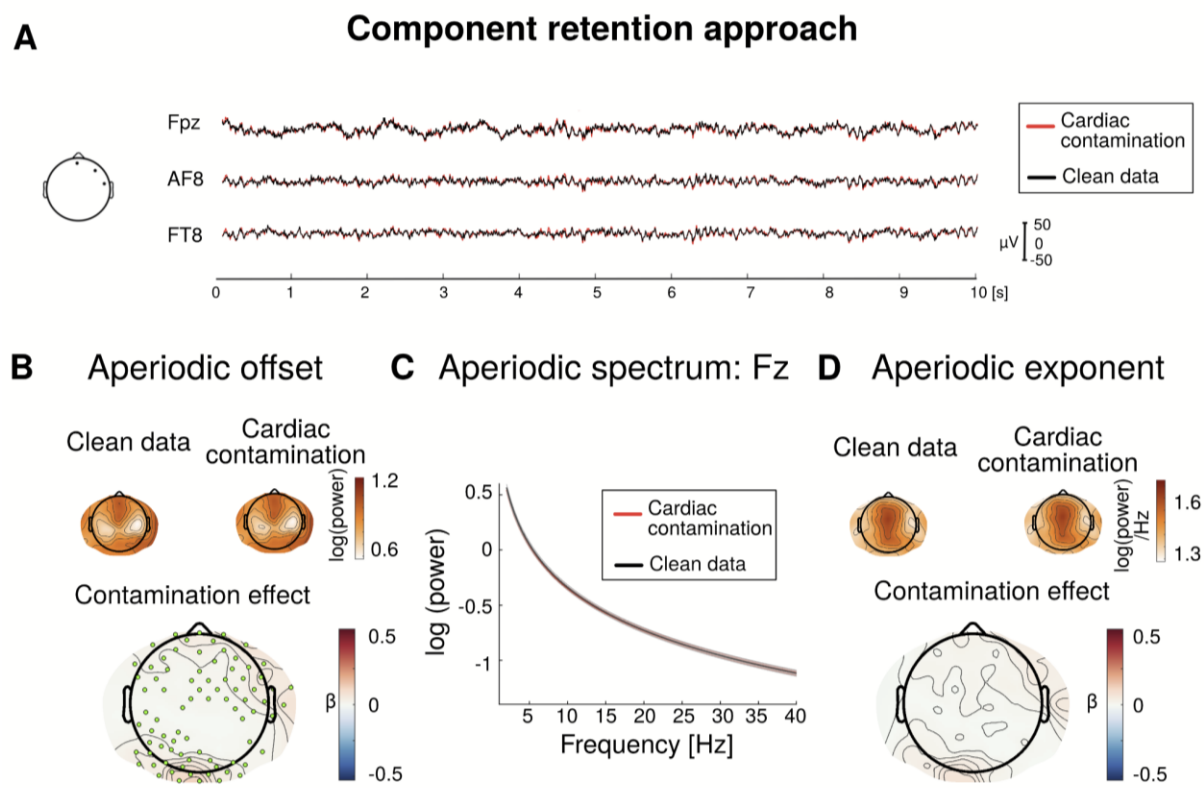

Figure 5: Effects of cardiac artifact contamination on aperiodic parameter estimation. Results are shown for the main dataset. Panel A shows prototypical data from three frontotemporal electrodes (from midline to right: Fpz, AF8 and FT8) before and after removal of ICs identified as cardiac activity. Small topographies above B and D display aperiodic parameters derived from fully cleaned data (all artifactual ICs removed) and partially cleaned data (cardiac ICs retained). Larger maps below show standardized regression coefficients from the linear mixed effects models, predicting the aperiodic parameters from cardiac contamination; Green dots mark significant electrodes in CBPT. Panel C shows mean aperiodic spectra for fully cleaned data and of data in which cardiac ICs were retained, with shaded areas indicating standard errors of the mean.

Result summary

Together, our analyses show that both the aperiodic offset and exponent are highly sensitive to EEG recording quality and physiological artifacts. Figure 6 summarizes these effects as standardized β values averaged across all electrodes, providing an overall estimate of the impact of data quality and artifact contamination on aperiodic parameters. The summary plot

further highlights the high consistency across analytic approaches (component retention and incremental contamination) and across datasets.

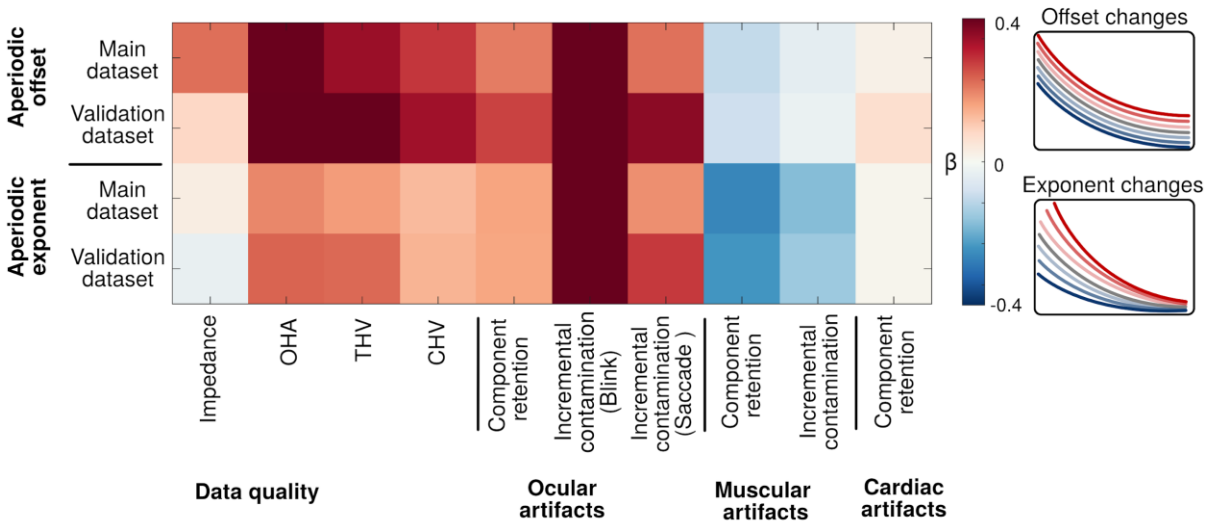

Figure 6: Average standardized β's of the linear models across all scalp electrodes. For the component retention approach, the β estimates reflect the contrast between artifact ICs retained vs. removed. For the incremental contamination approach, β estimates represent the contrast between medium contamination (i.e. 3 out of 15 segments contaminated) and clean data segments only. Note that average β estimates for the incremental blink contamination reached values up to 0.87, for OHA and THV up to 0.50. Schematic plots on the right illustrate how these reported beta estimates correspond to changes in each aperiodic parameter.

Mitigating artifact-induced biases through statistical correction

To illustrate a practical solution for cases where populations or experimental conditions differ systematically in artifact rates (e.g. comparing typical developing children and children with an ADHD diagnosis[31]), we conducted an additional analysis using the main dataset. We simulated a plausible scenario comparing populations with different levels of ocular contamination: 20% artifactual segments, representative of healthy populations[27], versus 40%, typical in clinical samples[27,31]. We focused on the aperiodic exponent, as it is more commonly studied than the offset[9,17].

The main dataset was randomly divided into two subgroups, and differential eye blink contamination was introduced using the incremental contamination approach (Figure 7A). Subgroup 1 consistently received low contamination (mean 3 contaminated segments of 15 total, normally distributed). Subgroup 2 was sampled twice, once under low contamination (Group 2A, identical to Subgroup 1) and once under high contamination condition (Group 2B, mean 6 of 15 segments, normally distributed). Aperiodic exponents were extracted at electrode POz from fully cleaned data (i.e., after removal of all artifactual ICs). The sampling strategy is shown in Fig. 7A, and the resulting contamination levels and exponent distributions in Fig. 7B.

As expected, groups with matched contamination levels (Group 1 vs. Group 2A) showed no significant difference in aperiodic exponents ($\beta < 0.001$, $p = 0.95$), whereas low versus high contamination groups differed significantly (Group 1 vs. Group 2B, $\beta = 0.11$, $p = 0.04$, Figure 7B, middle panel). Crucially, after regressing out the number of contaminated segments (residualizing the aperiodic exponent by contamination level), the group difference disappeared (Group 1 vs Group 2B, $\beta = 0.01$, $p = 0.81$), Figure 7B, bottom).

These results demonstrate that regression-based statistical correction effectively mitigates artifact-induced biases in aperiodic parameter comparisons. When populations or conditions differ systematically in artifact rates, quantifying and statistically controlling for these differences enables valid inference while maintaining statistical power.

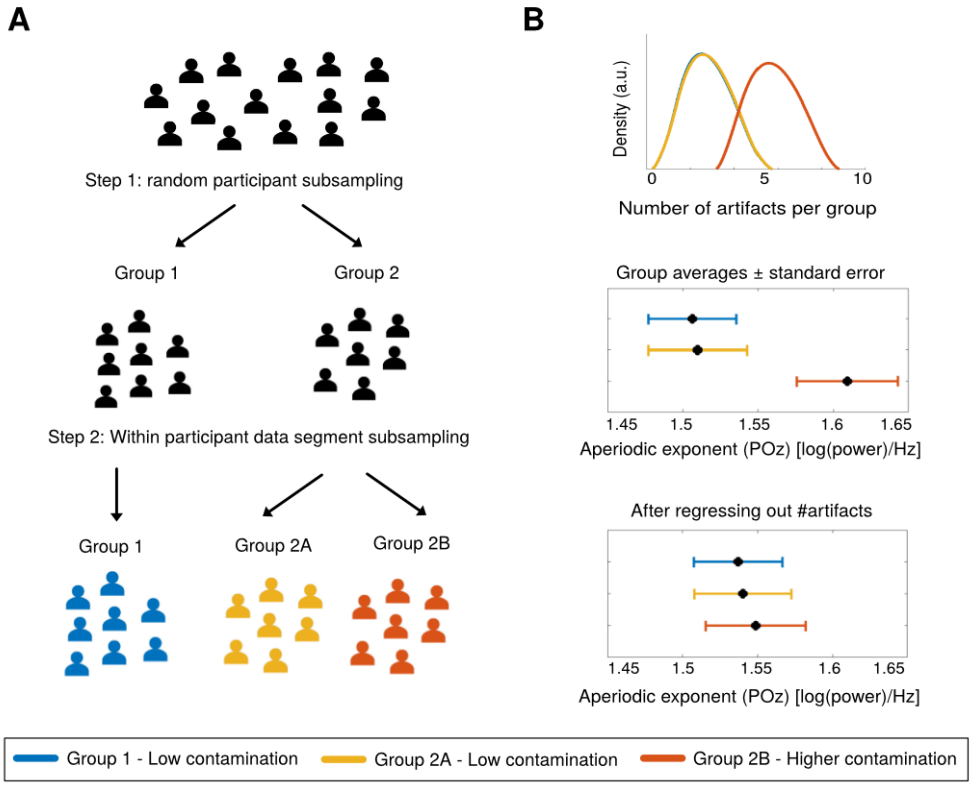

Figure 7: Statistical correction of artifact-induced biases in aperiodic parameters. Example shown for the effect of eye blinks on the parieto-occipital aperiodic exponent, based on fully cleaned data (all artifact ICs removed). Panel A shows the random subsampling of participants in the main dataset. Panel B displays artifact segments per subgroup (top) and the resulting aperiodic exponent estimates (bottom) plotted as group means ± standard error, before (upper) and after (lower) regressing out the number of artifacts.

Discussion

Our comprehensive analyses revealed that both data quality and physiological artifacts substantially affect aperiodic parameter estimation. Distinct directional patterns emerged across artifact types: poor data quality, ocular activity, and cardiac artifacts were associated with larger offsets and exponents (i.e., steeper aperiodic slopes), whereas muscular artifacts produced the opposite pattern (i.e., smaller offsets and flatter aperiodic slopes). Importantly, these effects were not confined to local regions but extended across the entire scalp, indicating that artifact sources influence aperiodic estimates even at distant electrodes. Crucially, these

effects persisted after applying state-of-the-art preprocessing at realistic contamination levels, suggesting that typical artifact correction procedures may not fully remove non-neural contributions from aperiodic parameters. Moreover, the magnitude of these influences was comparable to group differences often interpreted as physiologically meaningful in prior literature, underscoring their potential to bias neural inferences. The high consistency of results across two independent datasets and analytical approaches further demonstrates that these artifact-related effects on aperiodic parameters are robust and generalizable rather than system- or method-specific.

To understand the mechanisms underlying these effects, it is essential to consider how contamination sources interact with the parameter estimation algorithm. Each artifact type has distinct spectral characteristics that influence the aperiodic parameter estimation in specific ways. As pointed out by a previous study[36], oscillatory peaks near the lower or upper bound of the fitted frequency ranges can bias the estimation of the aperiodic parameters in specparam, but also in an alternative estimation method such as irregular-resampling autospectral analysis (IRASA[37]). Because non-neural artifacts typically exhibit high amplitudes, they are particularly susceptible to such misestimation.

This framework clarifies our findings: Ocular artifacts introduce high-amplitude low-frequency activity into the EEG signal[38,39], primarily affecting the lower end of the frequency spectrum used for aperiodic fitting (2-40 Hz) and thereby increasing both the aperiodic offset and exponents. In contrast, muscular artifacts produce high-frequency activity[34], elevating power near the upper bound of the fitting range (~40Hz) and consequently resulting in smaller offsets and exponents. Cardiac artifacts exerted more modest effects, likely reflecting the comparatively weak field strength of cardiac signals at the scalp. Poor data recording quality often reflect elevated low-frequency noise[40], yielding larger aperiodic offsets and steeper aperiodic signal components. Together, these observations highlight that aperiodic parameter estimation is vulnerable to systematic bias when non-neural sources introduce spectral power

that interferes with typical fitting ranges applied to the algorithm, challenging the presumed independence of periodic and aperiodic components.

Therefore, our findings have important implications for both basic EEG research and clinical applications. Although the component retention approach was designed to assess artifact contamination effects, it also revealed that ICA-based artifact correction substantially reduces contamination effects on aperiodic parameters, underscoring its value in preprocessing pipelines.

However, residual influences can persist even after state-of-the-art preprocessing, posing a risk for studies comparing populations or experimental conditions. Observed differences in the aperiodic parameters may be mistakenly interpreted as neural when they instead reflect variations in artifact prevalence. This concern is supported by prior work showing that observed age-related differences in aperiodic parameters were linked to cardiac activity, and that ICA-based rejection did not fully remove these effects[29]. Our results align and extend these observations, demonstrating that data quality and all major physiological artifact types (ocular, muscular, and cardiac) pose risks for misinterpretation in the anlyses of aperiodic activity. Such contamination challenges not only the interpretation of group differences as reflecting neural variation but also for theoretical frameworks that view population differences in the aperiodic exponent as evidence supporting the excitation-inhibition balance hypothesis. It is therefore essential to assess whether study groups or experimental conditions differ in data quality and artifact contamination. Across neuroimaging modalities, artifacts are consistently unevenly distributed across populations. For example, greater in-scanner head motion has been reported in ADHD[30,41], in ASD[30] and in schizophrenia[30] populations. Also EEG studies have found higher artifact rates in children and adolescents compared to adults, with further increases in pediatric ADHD[31], and elevated ocular artifacts have been demonstrated in schizophrenia patients compared to controls[42]. When such group differences exist, statistical control approaches can effectively mitigate bias. As demonstrated here (Figure 7), controlling for contamination levels effectively eliminates artifact-related influences,

helping to disentangle neural from non-neural contributions to aperiodic parameter differences.

While our findings provide systematic insights into the influence of artifacts on aperiodic parameter estimation and how such effects can be mitigated, several methodological limitations should be acknowledged. First, the efficacy of statistical correction depends on accurate artifact identification. Although our study benefited from eye-tracking for ocular artifacts and EMG validation for muscular artifact detection, automated classification accuracy may vary across populations, and many datasets lack auxiliary recordings for reliable artifact identification. Developing standardized artifact detection protocols therefore represents a crucial step toward ensuring the validity of aperiodic parameter analyses across diverse populations and research contexts.

Second, although ICA-based artifact correction is standard practice, components labeled as artifacts may also contain neural signals, potentially biasing results from the component retention approach. This risk may be amplified when using automated classifiers (e.g., ICLabel), even though automation enhances objectivity and reproducibility. However, the strong convergence with our incremental contamination analyses, which avoided ICA-based removal entirely, suggests that any potential neural signal loss did not drive the observed effects.

Finally, our analyses focused on specparam, which may limit generalizability to alternative aperiodic parameterization methods. However, specparam was chosen because it is the most widely used approach for aperiodic parameter estimation in the field[9,17]. Other approaches, such as IRASA, rely on different modeling principles and may show some method-specific variation.

Looking ahead, future studies should extend our findings to alternative parametrization approaches and beyond resting-state data, assessing artifact influences across diverse experimental paradigms, e.g. when tracking temporal dynamics of the aperiodic signal as

proposed in Wilson et al[43]. Most importantly, future work should systematically evaluate the extent to which previously reported aperiodic findings may have been affected by artifact contamination, determining whether observed group differences, developmental trajectories, and experimental effects remain significant after controlling for differential artifact rates.

In conclusion, our findings demonstrate that data quality and physiological artifacts introduce systematic biases in aperiodic signal parameters, with magnitudes comparable to those often interpreted as meaningful neurophysiological effects. Although state-of-the-art preprocessing can attenuate these biases, they may still influence reported group or condition differences. As aperiodic parameters gain prominence in studies of brain function across development, aging, and clinical populations, recognizing and statistically controlling for these contamination sources will be essential. Implementing such practices will allow researchers to disentangle neural mechanisms from methodological confounds, strengthen the validity of between-group comparisons, and advance a more precise understanding of the neural processes reflected in the aperiodic signal component.

Methods

Datasets

All analyses were conducted on a main and an independent validation dataset to enhance the robustness of our results, and evaluate their generalizability across different EEG systems. In both datasets, EEG and eye tracking data were collected simultaneously during resting state recordings. In the main dataset, which was specifically recorded for the purpose of this study, additional ECG and EMG channels were included to improve the identification of physiological artifacts. The following sections describe each dataset and the corresponding EEG hardware used for data acquisition.

Main dataset

The main dataset comprised 99 healthy young participants aged 18-35 years. Individuals were excluded if they exhibited psychiatric symptoms, suffered from severe neurological disorders or if they currently used psychotropic drugs such as antidepressants, alpha-agonists, neuroleptics and mood stabilizers, or recreational drugs. The study was approved by the ethics committee of the Faculty of Arts and Social Sciences of the University of Zurich, and all participants provided written informed consent.

Main dataset: Data acquisition

For the main dataset, EEG was acquired using a 128-channel ANT Neuro system (ANT Neuro, Hengelo, Netherlands) with a sampling rate of 500Hz. Recordings were referenced to CPz, and impedances were maintained below 20 kΩ. In addition to the EEG channels, a horizontal and vertical electrooculogram (EOG), three bipolar EMG channels, and a two-electrode electrocardiogram were obtained with the same sampling rate of 500Hz. The EMG electrode pairs were placed above the left eyebrow, on the left cheek (above the masseter muscle), and on the right upper neck (to capture activity of the trapezius and the sternocleidomastoid

muscle). Electrode locations were selected following prior work capturing EMG activity in the context of EEG recordings[44]. For the ECG, one electrode was placed in the right infraclavicular area (below the clavicle at the midclavicular line) and the other on the left lower torso, near the iliac crest. EEG and ECG were recorded with a common ground, positioned on the right mastoid. Eye movements were simultaneously recorded by an infrared video-based eye tracker (EyeLink 1000 Plus, SR Research) at a sampling rate of 500 Hz and an instrumental spatial resolution of 0.01°.

Validation dataset

The second employed validation dataset was previously recorded in our laboratory and comprised 103 healthy participants aged 18–35 years. The same exclusion criteria as for the main dataset were applied here. The study was approved by the Institutional Review Board of Canton Zurich (BASEC-Nr. 2017–00226), and all participants provided written informed consent.

Validation dataset: Data acquisition

EEG data was recorded at a sampling rate of 500 Hz using a 128-channel EEG Geodesic Sensor Net system (Electrical Geodesics, Eugene, Oregon). Recordings were referenced to Cz (vertex of the head), and electrode impedances were kept below 40 kΩ. Additionally, eye movements were recorded by the same infrared video-based eye tracker as in the main dataset (EyeLink 1000 Plus, SR Research).

Experimental setup and procedure

Identical procedures were used for the collection of both datasets. Participants were seated in a sound- and electrically shielded Faraday cage, equipped with a 24-inch screen (ASUS ROG Swift PG248Q, resolution 800 × 600 pixels) and a chinrest positioned 68cm from the screen. Resting-state recordings were obtained immediately after electrode preparation (i.e.,

impedances were below 20 kΩ in the main dataset or 40 kΩ in the validation dataset) and the calibration of the eye tracker. The eye tracker calibration and validation were performed on a 9-point grid until the average validation error across all points was <1°.

Resting-state EEG data was recorded while participants alternated between eyes-open and eyes-closed conditions. Audio cues delivered through in-cage loudspeakers indicated the transitions between the conditions. Following an established protocol[45,46], participants completed five cycles, each consisting of 20 s of eyes-open fixation followed by 40 s of eyes-closed rest, yielding a total of 100 s of eyes-open and 200 s of eyes-closed data for analysis.

Preprocessing

The same preprocessing pipeline was applied to the full resting-state recordings of both datasets, including the alternating eyes-open and eyes-closed periods. In the main dataset, the auxiliary electrodes (EOG, ECG, EMG) were excluded from the below described preprocessing steps to preserve their raw signals, however they were included for the ICA decomposition to improve the identification of ocular, cardiac and muscular artifact ICs.

Because the primary focus of this study was to examine the influence of data quality and physiological artifacts on estimates of the aperiodic signal, preprocessing followed a state-of-the-art pipeline to mirror realistic research practice. Therefore, the automated preprocessing toolbox Automagic[47] was employed, which performed detection and interpolation of bad channels, a 0.5 Hz high pass filter and line noise removal (“Basic preprocessing"; Figure 1).

Independent component analysis (ICA) was then performed. To allow for subsequent analyses of selective artifact removal and retention (see below), all ICs were retained in the data. For the pipeline’s automated data-quality assessment, however, artifactual ICs (classified by ICLabel) were temporarily removed. Datasets rated as poor quality were excluded from further processing (see Supplement 7 for a detailed description of the pipeline). Before the final

extraction of the aperiodic signal component, data was rereferenced to the common average reference.

For all analyses, except the incremental contamination analysis on ocular artifacts (see below), data from the eyes-closed condition were used, which is most commonly employed in resting state EEG studies[48]. Therefore, data of the five 40-second segments were concatenated. The first and last two seconds of each segment were excluded to remove potential artifacts of the acoustic prompts and of eyes closure or eyes opening, respectively, yielding a total of 180 seconds of eyes-closed data. For the eyes-open data, a total of 80 seconds was available after merging and applying the same exclusions.

Calculation of the aperiodic signal component

For all analysis approaches outlined below, the aperiodic parameters were calculated as follows. The power spectral density (PSD) was first computed using Welch's Method[49], with a window length of 1 second. The resulting PSD was then parameterized using the specparam algorithm[1], which decomposes the power spectrum into an aperiodic component and oscillatory peaks. In brief, the algorithm iteratively models the PSD as an aperiodic component (L) and a set of Gaussians representing oscillatory peaks rising above the aperiodic signal. A detailed description of the fitting procedure is provided in Donoghue et al.[1]

The aperiodic component is defined as:

$$L = b - log\,(k + F^{\chi})$$

Here, b represents the aperiodic offset, F, the vector of input frequencies, and χ the aperiodic exponent. The additional k parameter is set to 0 in the present analysis, as this parameter allows to model a bend of the aperiodic component which is primarily needed when fitting signals in broad frequency ranges, typically in intracranial recordings[2]. Further settings for the

algorithm were: peak width limits: [1, 8]; max number of peaks: infinite; minimum peak height: 0; peak threshold: 2 sd above mean. The model was fitted to a frequency range of 2-40 Hz, consistent with the original specparam algorithm publication[1]. Furthermore, this range was commonly used in subsequent studies examining the relationship between aperiodic activity and age[13,14,50–52] and was most frequently applied in clinical investigations on aperiodic parameters[9].

Across all analytic subsamples, the specparam algorithm achieved consistently high model fits across (R^2 = 0.96-0.99), regardless of differences in EEG data quality and artifact contamination levels between approaches (see Supplement 8 for a detailed assessment of model fits across analyses).

Effect of data quality on the aperiodic signal

As depicted in Figure 1 (green box), analyses of the relationship between data quality and the aperiodic signal parameters were conducted on fully cleaned data (i.e. after removal of all artifactual ICs). This approach was chosen to mirror a realistic scenario, enabling us to assess whether the quality of data acquisition influences the estimated aperiodic parameters even after state-of-the-art preprocessing.

Hardware based quality metrics: Electrode impedances

As a first measure of recording quality, electrode impedances were extracted. In both study protocols (i.e. in the main and the validation dataset), impedances were recorded immediately after electrode preparation by the research assistants. Because the resting-state paradigm was always the first to be collected, impedance measures corresponded to the beginning of the analyzed EEG recordings. For subsequent statistical analyses, only impedance values

within ranges commonly accepted in EEG research were included. Following the recommendation of the EEG system manufacturers, the cut-off was set to 20 kΩ for main dataset (electrolyte gel-based EEG system), and to 50 kΩ for the validation dataset (salt water-based EEG system). The distribution of electrode impedances is shown in Supplement 9.

Algorithmic quality metrics

The second analysis examined the relationship between the aperiodic signal parameters and objective, algorithmic estimates of data quality, assessed at the end of the preprocessing pipeline (i.e.after temporal removal of all artifactual ICs). Whereas the thresholded version of these quality metrics were used during preprocessing to exclude bad quality data (see section "Preprocessing" and Supplement 7), here we used their continuous values. In more detail, these metrics were defined as described and validated in Pedroni et al.[47]: Ratio of data with overall high amplitude (OHA), defined as the ratio of datapoints (i.e. channels × timepoints) that have an absolute voltage value larger than 20 μV. Ratio of timepoints of high variance (THV) measures the ratio of time points where the standard deviation across channels exceeds 10 μV. Ratio of channels of high variance (CHV), the final measure, is defined as the ratio of channels whose standard deviation across all timepoints exceeds 10 μV. Unlike electrode impedances, which are measured individually for each electrode, these three algorithmic quality metrics each yield a single summary value for the entire EEG recording. Distributions of the three quality metrics are provided in Supplement 9.

Relationships among all quality measures are evaluated in Supplement 10. In brief, electrode impedances and algorithmic metrics were largely uncorrelated and thus reflect distinct aspects of data quality, whereas the three algorithmic metrics showed high intercorrelations, indicating substantial overlap, but still accounting for partly distinct variance components.

Effect of physiological artifacts on the aperiodic signal component

The second set of analyses investigated the influence of physiological artifacts on the estimated aperiodic parameters (Figure 1, blue boxes). Two complementary approaches were employed: *component retention* and *incremental contamination*. The following sections describe each in more detail.

Component retention approach

This approach assessed the impact of physiological artifact contamination by comparing the aperiodic signal estimated on EEG data while either retaining or removing ICs representing non-neural activity. Probability scores assigned by ICLabel during preprocessing were used for classification. In a first step, all ICs reflecting artifacts (ocular, muscular, cardiac, line noise, channel noise) with probabilities >0.8 were removed from the data and the aperiodic signal was estimated based on this cleaned dataset (i.e. “fully cleaned data”). Next, to isolate the effect of specific artifact types, the IC removal procedure was repeated in three separate iterations. In each iteration all artifactual ICs were removed except those of a single target class (e.g., ocular ICs retained; see Fig. 1 for a visualization). After each selective retention, the aperiodic signal was re-estimated, thereby enabling assessment of the influence of that artifact category on the aperiodic parameters. Supplement 2 visualizes the number of ICs for each artifact category per participant.

In line with typical resting-state paradigms, these analyses were conducted on the merged eyes-closed EEG data. Importantly, eye movements continue to occur under lid closure, even when participants are instructed to maintain a given position of the eye[53]. However, for supplementary analysis, the effect of ocular artifact contamination was also estimated on eyes-open resting state data.

Incremental contamination approach

Because ICA cannot perfectly separate neural from non-neural signals, we implemented an alternative approach to complement the component retention approach. This second approach was designed to reduce the risk that removing ICs identified as artifacts would also eliminate neural activity and thereby affect the estimated aperiodic parameters. Consequently, instead of relying on ICA-based artifact correction, the aperiodic parameters were estimated either from entirely artifact-free segments only, or from segments that intentionally included varying levels of artifact contamination. In a first step, two algorithms (described below) were applied to the basic preprocessed resting-state EEG data (i.e. prior to IC removal) to identify segments containing physiological artifacts. In a next step, 15 artifact-free one-second segments were extracted, and the aperiodic parameters were calculated on these clean segments. Subsequently, either one, three or five of the clean segments were exchanged with artifact-contaminated segments of the same length, and the aperiodic parameters were recalculated for each configuration (see Figure 1 for a visualization). Only participants were included, who had at least 15 clean segments, and five segments containing artifacts respectively. The number of 15 clean segments was chosen to balance participant retention with sufficient model fit quality for the specparam algorithm (see Supplement 2). The chosen contamination levels (~7%, 20%, and 33%) reflect typical ranges of artifact contamination in EEG data, which often vary between 20–40% depending on the investigated population[27,31]. The full distribution of the number of available segments per subject is presented in Supplementary 2.

For supplementary analyses, artifact-contaminated time windows (identified in the basic preprocessed data) were used to extract corresponding segments from the fully cleaned EEG (i.e., after removal of all artifactual ICs, as described above). This allowed us to assess whether residual effects of physiological artifacts on the aperiodic parameter estimation persisted after state-of-the-art artifact correction.

The following two sections describe how segments containing ocular and muscular artifacts were determined.

Ocular artifacts

To examine the influence of saccades and blinks on the aperiodic signal parameters, the incremental contamination approach was applied to merged eyes-open resting-state data. Using eyes-open data allowed us to incorporate eye tracking information as a ground truth to identify segments containing ocular artifacts. EEG and eye-tracking data were co-registered with the EYE-EEG toolbox[54]. Artifact-free segments were defined as one-second EEG epochs during fixation periods (i.e., during periods of no eye movement) as indicated by the eye tracker. From these, 15 segments were randomly selected. Segments containing blinks were identified by epoching around blink onsets (–200 to +800 ms), detected by the eye tracker. From all potential segments containing a blink, either one, three or five segments were randomly selected. Likewise, segments containing saccades were determined by segmenting around saccade events.

Muscular artifacts

Muscular artifacts during merged eyes-closed resting-state recordings were identified using two complementary algorithms. The first artifact detection algorithm was based on EEG data and thus could be applied to both the main and the validation dataset. To obtain a more direct measure of muscular activity, three bipolar EMG channels were additionally recorded in the main dataset (see above). Based on these electrodes, a second algorithm was implemented to identify segments containing muscular artifacts.

The EEG-based muscular artifact detection was performed using a state-of-the-art procedure[34]. Specifically, the first principal component of the EEG data, which typically contains high amplitude artifacts[55], was extracted. This component was then filtered to higher

frequency bands (65-115Hz) to enhance muscular contributions, and its envelope was low pass filtered (4Hz) to remove transient noise peaks. This signal was finally thresholded to detect artifact segments (see Supplement 11 for a detailed description).

For the main dataset, EMG-based muscular artifact detection was performed on the three bipolar EMG channels. Signal envelopes were computed for each EMG channel (also low-passed filtered at 4 Hz to suppress transient noise peaks) and thresholded to detect muscular activity whenever any of the three processed channels exceeded the criterion (see Supplement 11 for details).

Statistical analysis

Prior to statistical analyses, all continuous variables were z-transformed to standardize the regression coefficients, enabling direct interpretation of the resulting estimates in terms of effect size. To account for the problem of multiple comparisons across electrodes (105 or 128 channels, depending on dataset), cluster-based permutation tests (CBPTs) as implemented in FieldTrip[56], in combination with custom-written functions, were employed.

Data quality: Linear models & cluster-based permutation tests

To statistically evaluate the relationship between the aperiodic l parameters and the measures of data quality (i.e. electrode impedances and the algorithmic quality metrics CHV, THV and OHA), we fitted the following linear models:

$$aperiodic\ parameter \sim data\ quality\ metric$$

Note that the models were fitted for each quality metric independently and separately for the aperiodic offset and exponent. Spatial clusters were defined by thresholding the t-values of the β coefficient at a two-tailed $p < 0.05$ (i.e., t-values exceeding the critical t for $p = 0.025$ in each tail), and grouping neighboring electrodes showing significant t-values. Next, the t-statistics within each cluster were summed to calculate cluster-mass statistics ("maxsum"

method). To generate the null distribution, 1000 permutations were performed by randomly shuffling data quality values across participants; for each permutation, the maximum cluster mass of the largest identified cluster was retained. A cluster in the observed data was deemed significant if its mass exceeded the 97.5th percentile of the permutation distribution of cluster masses (cluster-level α = .025, adjusted for two tails).

Physiological artifacts: Linear mixed effects models & cluster-based permutation tests

To evaluate whether physiological artifact contamination influenced the estimated aperiodic signal parameters, similar CBPTs statistics were applied using linear mixed-effects models. Note that separate models were fitted for the aperiodic offset and the aperiodic exponent. For the component retention approach, the following model was applied:

$$aperiodic\ \ parameter \sim component\ retention\ + (1 \mid subjectID)$$

where the factor "component retention" indicated whether artifact-related ICs were removed (0) or retained (1). In this case, statistical inference was based on the fixed-effect t-statistics associated with the *component retention* predictor as provided by the linear mixed-effects model. These t-statistics were used as the input for cluster formation in the CBPT.

For the incremental contamination approach, the model was defined as:

$$aperiodic\ \ parameter \sim artifact\ contamination\ +\ (1 \mid subjectID)$$

Here, the *artifact contamination* factor had four levels: 0 (clean data segments only), 1 = low contamination (1 artifactual segment), 2 = medium contamination (3 artifactual segments) and 3 = high contamination (5 artifactual segments). Random intercepts for subjects were included in both models to account for within-subject dependencies across repeated conditions.

For the incremental contamination analysis, test statistics were derived using a model comparison framework. Specifically, likelihood ratio tests were conducted between each full model and a reduced baseline model:

$$aperiodic\ parameter \sim 1 + (1 \mid subjectID)$$

This model comparison approach was used to obtain a single test statistic reflecting the overall effect of the artifact factor, which can be employed for cluster formation, rather than performing separate CBPTs for each individual factor level. The likelihood ratio test statistic approximates a chi-square distribution, therefore, cluster formation is based on extreme values in this distribution at an alpha level of 0.05. Note that the likelihood-ratio test evaluates only whether the full model with the additional factor (i.e *artifact contamination*) provides a significantly better fit than the reduced model. Thus, the resulting statistic tests a single directional hypothesis (improvement in fit), and is therefore a one-sided test (i.e. the α level of 0.05 was not further divided).

As described for the analysis on data quality, the sum of the test statistics in each formed cluster is saved for the observed data, and compared to a null distribution based on 1000 permutations of randomly shuffled factor levels within participants. Again, a cluster was deemed significant if its observed mass exceeded the 97.5th percentile of the permutation distribution (cluster-level α = .025, adjusted for two tails).

Data availability

All data that support the findings of this study are available on: https://gin.g-node.org/mtroen/NonNeuralAperioidic

Code availability

All analysis code is available on a public repository: https://gin.g-node.org/mtroen/NonNeuralAperioidic

Competing interests

The authors declare no competing interests.

Author contributions

M.T. contributed: Writing – original draft, Methodology, Formal analysis, Data curation, Conceptualization

N.L. contributed: Writing – review & editing, Supervision, Project administration, Methodology, Formal analysis, Conceptualization.

References

1. Donoghue, T. *et al.* Parameterizing neural power spectra into periodic and aperiodic components. *Nat. Neurosci.* **23**, 1655–1665 (2020).
2. Miller, K. J., Sorensen, L. B., Ojemann, J. G. & Nijs, M. den. Power-Law Scaling in the Brain Surface Electric Potential. *PLOS Comput. Biol.* **5**, e1000609 (2009).
3. Manning, J. R., Jacobs, J., Fried, I. & Kahana, M. J. Broadband Shifts in Local Field Potential Power Spectra Are Correlated with Single-Neuron Spiking in Humans. *J. Neurosci.* **29**, 13613–13620 (2009).
4. Voytek, B. *et al.* Age-Related Changes in 1/ *f* Neural Electrophysiological Noise. *J. Neurosci.* **35**, 13257–13265 (2015).
5. Voytek, B. & Knight, R. T. Dynamic Network Communication as a Unifying Neural Basis for Cognition, Development, Aging, and Disease. *Biol. Psychiatry* **77**, 1089–1097 (2015).
6. Bak, P., Tang, C. & Wiesenfeld, K. Self-organized criticality: An explanation of the 1/ *f* noise. *Phys. Rev. Lett.* **59**, 381–384 (1987).
7. He, B. J. Scale-free brain activity: past, present, and future. *Trends Cogn. Sci.* **18**, 480–487 (2014).
8. Hidalgo, J. *et al.* Information-based fitness and the emergence of criticality in living systems. *Proc. Natl. Acad. Sci.* **111**, 10095–10100 (2014).
9. Donoghue, T. A systematic review of aperiodic neural activity in clinical investigations. 2024.10.14.24314925 Preprint at https://doi.org/10.1101/2024.10.14.24314925 (2024).
10. Brake, N. *et al.* A neurophysiological basis for aperiodic EEG and the background spectral trend. *Nat. Commun.* **15**, 1514 (2024).
11. Gao, R., Peterson, E. J. & Voytek, B. Inferring synaptic excitation/inhibition balance from field potentials. *NeuroImage* **158**, 70–78 (2017).
12. Hill, A. T., Clark, G. M., Bigelow, F. J., Lum, J. A. G. & Enticott, P. G. Periodic and aperiodic neural activity displays age-dependent changes across early-to-middle

childhood. *Dev. Cogn. Neurosci.* **54**, 101076 (2022).

13. Tröndle, M., Popov, T., Dziemian, S. & Langer, N. Decomposing the role of alpha oscillations during brain maturation. *eLife* **11**, e77571 (2022).
14. Tröndle, M. *et al.* Decomposing age effects in EEG alpha power. *Cortex* **161**, 116–144 (2023).
15. Frelih, T., Matkovič, A., Mlinarič, T., Bon, J. & Repovš, G. Modulation of aperiodic EEG activity provides sensitive index of cognitive state changes during working memory task. Preprint at https://doi.org/10.1101/2024.05.13.593835 (2024).
16. Virtue-Griffiths, S. *et al.* Task-related changes in aperiodic activity are related to visual working memory capacity independent of event-related potentials and alpha oscillations. Preprint at https://doi.org/10.1101/2022.01.18.476852 (2022).
17. Hemmerich, K., Santoni, A., Stottmeier, S. & Ronconi, L. Aperiodic EEG features of cognition: A systematic review. Preprint at https://doi.org/10.31234/osf.io/m2n6r_v1 (2025).
18. Leno, V. C. *et al.* Cortical markers of excitation/inhibition balance are associated with sensory responsivity from infancy in longitudinal cohorts enriched for autism and ADHD. Preprint at https://doi.org/10.21203/rs.3.rs-3879380/v1 (2024).
19. Shuffrey, L. C. *et al.* Aperiodic electrophysiological activity in preterm infants is linked to subsequent autism risk. *Dev. Psychobiol.* **64**, e22271 (2022).
20. Molina, J. L. *et al.* Memantine Effects on Electroencephalographic Measures of Putative Excitatory/Inhibitory Balance in Schizophrenia. *Biol. Psychiatry Cogn. Neurosci. Neuroimaging* **5**, 562–568 (2020).
21. Peterson, E. J., Rosen, B. Q., Belger, A., Voytek, B. & Campbell, A. M. Aperiodic Neural Activity is a Better Predictor of Schizophrenia than Neural Oscillations. *Clin. EEG Neurosci.* **54**, 434–445 (2023).
22. Dakwar-Kawar, O. *et al.* Aperiodic and periodic components of oscillatory brain activity in relation to cognition and symptoms in pediatric ADHD. *Cereb. Cortex* **34**, bhae236 (2024).

23. Robertson, M. M. *et al.* EEG power spectral slope differs by ADHD status and stimulant medication exposure in early childhood. *J. Neurophysiol.* **122**, 2427–2437 (2019).
24. Wang, Z. *et al.* The effect of aperiodic components in distinguishing Alzheimer's disease from frontotemporal dementia. *GeroScience* **46**, 751–768 (2023).
25. Rosenblum, Y. *et al.* Decreased aperiodic neural activity in Parkinson's disease and dementia with Lewy bodies. *J. Neurol.* **270**, 3958–3969 (2023).
26. Norouzi, H., Ietswaart, M., Adair, J. & Learmonth, G. A meta-analysis of periodic and aperiodic M/EEG components in Parkinson's disease. Preprint at https://doi.org/10.1101/2025.07.07.663454 (2025).
27. Luck, S. J. *An Introduction to the Event-Related Potential Technique*. (The MIT Press, Cambridge, Massachusetts, 2014).
28. Tiwari, A. *et al.* On the Use of FOOOF for Electroencephalography Quality Measurement and Device Assessment. in *2023 IEEE International Conference on Systems, Man, and Cybernetics (SMC)* 4746–4751 (IEEE, Honolulu, Oahu, HI, USA, 2023). doi:10.1109/SMC53992.2023.10394590.
29. Schmidt, F. *et al.* Age-related changes in "cortical" 1/f dynamics are linked to cardiac activity. *eLife* **13**, (2025).
30. Pardoe, H. R., Kucharsky Hiess, R. & Kuzniecky, R. Motion and morphometry in clinical and nonclinical populations. *NeuroImage* **135**, 177–185 (2016).
31. Kaiser, A. *et al.* EEG Data Quality: Determinants and Impact in a Multicenter Study of Children, Adolescents, and Adults with Attention-Deficit/Hyperactivity Disorder (ADHD). *Brain Sci.* **11**, 214 (2021).
32. Bai, D., Guo, Y., Jülich, S. & Lei, X. Aperiodic and periodic components of resting-state EEG in primary insomnia. *Sleep Med.* **129**, 45–54 (2025).
33. Pion-Tonachini, L., Kreutz-Delgado, K. & Makeig, S. ICLabel: An automated electroencephalographic independent component classifier, dataset, and website. *NeuroImage* **198**, 181–197 (2019).
34. Gerla, V. *et al.* Automatic identification of artifacts and unwanted physiologic signals in

EEG and EOG during wakefulness. *Biomed. Signal Process. Control* **31**, 381–390 (2017).

35. Nanchen, D. Resting heart rate: what is normal? *Heart* **104**, 1048–1049 (2018).
36. Gerster, M. *et al.* Separating Neural Oscillations from Aperiodic 1/f Activity: Challenges and Recommendations. *Neuroinformatics* **20**, 991–1012 (2022).
37. Wen, H. & Liu, Z. Separating Fractal and Oscillatory Components in the Power Spectrum of Neurophysiological Signal. *Brain Topogr.* **29**, 13–26 (2016).
38. Noureddin, B., Lawrence, P. D. & Birch, G. E. Time-frequency Analysis of Eye Blinks and Saccades in EOG for EEG Artifact Removal. in *2007 3rd International IEEE/EMBS Conference on Neural Engineering* 564–567 (IEEE, Kohala Coast, HI, USA, 2007). doi:10.1109/CNE.2007.369735.
39. Bansal, Mahajan, D., Rashima, Singh, S., Rathee, D. & Roy, S. Real Time Acquisition and Analysis of Neural Response for Rehabilitative Control. *Int. J. Electr. Comput. Electron. Commun. Eng.* **8**, (2014).
40. Kappenman, E. S. & Luck, S. J. The effects of electrode impedance on data quality and statistical significance in ERP recordings. *Psychophysiology* https://doi.org/10.1111/j.1469-8986.2010.01009.x (2010) doi:10.1111/j.1469-8986.2010.01009.x.
41. Dziemian, S., Barańczuk-Turska, Z. & Langer, N. Association between attention-deficit/hyperactivity disorder symptom severity and white matter integrity moderated by in-scanner head motion. *Transl. Psychiatry* **12**, 434 (2022).
42. Gasser, T., Ziegler, P. & Gattaz, W. F. The deleterious effect of ocular artefacts on the quantitative EEG, and a remedy. *Eur. Arch. Psychiatry Clin. Neurosci.* **241**, 352–356 (1992).
43. Wilson, L. E., Da Silva Castanheira, J. & Baillet, S. Time-resolved parameterization of aperiodic and periodic brain activity. *eLife* **11**, e77348 (2022).
44. Li, Y. *et al.* Electromyogram (EMG) Removal by Adding Sources of EMG (ERASE)—A Novel ICA-Based Algorithm for Removing Myoelectric Artifacts From EEG. *Front.*

Neurosci. **14**, 597941 (2021).

45. Alexander, L. M. *et al.* An open resource for transdiagnostic research in pediatric mental health and learning disorders. *Sci. Data* **4**, 170181 (2017).
46. Langer, N. *et al.* A resource for assessing information processing in the developing brain using EEG and eye tracking. *Sci. Data* **4**, 170040 (2017).
47. Pedroni, A., Bahreini, A. & Langer, N. Automagic: Standardized preprocessing of big EEG data. *NeuroImage* **200**, 460–473 (2019).
48. Newson, J. J. & Thiagarajan, T. C. EEG Frequency Bands in Psychiatric Disorders: A Review of Resting State Studies. *Front. Hum. Neurosci.* **12**, (2019).
49. Welch, P. The use of fast Fourier transform for the estimation of power spectra: A method based on time averaging over short, modified periodograms. *IEEE Trans. Audio Electroacoustics* **15**, 70–73 (1967).
50. Cellier, D., Riddle, J., Petersen, I. & Hwang, K. The development of theta and alpha neural oscillations from ages 3 to 24 years. *Dev. Cogn. Neurosci.* **50**, 100969 (2021).
51. Hill, A. T., Clark, G. M., Bigelow, F. J., Lum, J. A. G. & Enticott, P. G. Periodic and aperiodic neural activity displays age-dependent changes across early-to-middle childhood. *Dev. Cogn. Neurosci.* **54**, 101076 (2022).
52. Merkin, A. *et al.* Do age-related differences in aperiodic neural activity explain differences in resting EEG alpha? *Neurobiol. Aging* **121**, 78–87 (2023).
53. Allik, J., Rauk, M. & Luuk, A. Control and Sense of Eye Movement behind Closed Eyelids. *Perception* **10**, 39–51 (1981).
54. Dimigen, O., Sommer, W., Hohlfeld, A., Jacobs, A. M. & Kliegl, R. Coregistration of eye movements and EEG in natural reading: Analyses and review. *J. Exp. Psychol. Gen.* **140**, 552–572 (2011).
55. Wallstrom, G. L., Kass, R. E., Miller, A., Cohn, J. F. & Fox, N. A. Automatic correction of ocular artifacts in the EEG: a comparison of regression-based and component-based methods. *Int. J. Psychophysiol.* **53**, 105–119 (2004).
56. Oostenveld, R., Fries, P., Maris, E. & Schoffelen, J.-M. FieldTrip: Open Source Software

for Advanced Analysis of MEG, EEG, and Invasive Electrophysiological Data. *Comput. Intell. Neurosci.* **2011**, 1–9 (2011).